Inorganic Chemistry

Article

pubs.acs.org/IC

Flexible Binding of PNP Pincer Ligands to Monomeric Iron Complexes

Kathlyn L. Fillman,[†,§] Elizabeth A. Bielinski,[‡,§] Timothy J. Schmeier,[‡] Jared C. Nesvet,[†] Tessa M. Woodruff,[†] Cassie J. Pan,[‡] Michael K. Takase,[‡] Nilay Hazari,*[,‡] and Michael L. Neidig*[,†]

[†]Department of Chemistry, University of Rochester, Rochester, New York 14627, United States

[‡]Department of Chemistry, Yale University, P.O. Box 208107, New Haven, Connecticut 06520, United States

Supporting Information

ABSTRACT: Transition metal complexes supported by pincer ligands have many important applications. Here, the syntheses of five-coordinate PNP pincer-supported Fe complexes of the type (PNP)$FeCl_2$ (PNP = $HN\{CH_2CH_2(PR_2)\}_2$, R = *i*Pr (^{iPr}PNP), *t*Bu (^{tBu}PNP), or cyclohexyl (^{Cy}PNP)) are reported. In the solid state, (^{iPr}PNP)$FeCl_2$ was characterized in two different geometries by X-ray crystallography. In one form, the ^{iPr}PNP ligand binds to the Fe center in the typical meridional geometry for a pincer ligand, whereas in the other form, the ^{iPr}PNP ligand binds in a facial geometry. The electronic structures and geometries of all of the (PNP)$FeCl_2$ complexes were further explored using ^{57}Fe Mössbauer and magnetic circular dichroism spectroscopy. These measurements show that in some cases two isomers of the (PNP)$FeCl_2$ complexes are present in solution and conclusively demonstrate that binding of the PNP ligand is flexible, which may have implications for the reactivity of this important class of compounds.

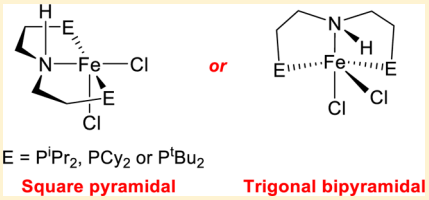

INTRODUCTION

Over the last two decades, pincer ligands have become some of the most versatile and important ligands for supporting reactive transition metal complexes.[1] In general, their straightforward and modular syntheses allow for relatively facile tuning of both the steric and electronic properties of pincer-supported complexes. Furthermore, the strong binding of these ligands to a variety of different metals often generates complexes with extremely high thermal stability. As a result, transition metal complexes supported by pincer ligands have been utilized for the activation of small molecules such as CO_2[2] and N_2[3] and as catalysts for a variety of processes including alkane dehydrogenation,[4] alkane metathesis,[4] olefin polymerization,[5] and transfer hydrogenation.[6] However, despite the impressive applications of pincer-supported complexes, the binding of pincer ligands to transition metals has not been explored to the same extent as the coordination of simple monodentate and bidentate ligands. Therefore, fundamental studies on the properties of pincer-supported transition metal complexes, which could provide insight for the design of the next generation of reactive species, are important.

In recent years, PNP-type pincer ligands of the general formula $HN\{CH_2CH_2(PR_2)\}_2$ (R = alkyl or aryl) have received significant attention.[7] They have been used both to stabilize transition metal catalysts and also to prepare complexes in unusual geometries. For example, Beller and co-workers[7ab,ac] have catalytically dehydrogenated methanol to H_2 and CO_2 using both Fe and Ru complexes supported by a PNP ligand, whereas Schneider has utilized this ligand to prepare the first examples of square planar Rh, Ru, and Ir nitrides.[7t,w,y] In almost all reported complexes supported by PNP ligands, the ligand binds in the expected meridional geometry for a pincer ligand. Nevertheless, there are a handful of examples, particularly in dimeric complexes, where the PNP ligand binds in a facial geometry.[7d,h,i,u] This has led to speculation that these ligands with alkyl linkers are flexible and that intermediates in reactions give different products depending on whether the ligand is in a meridional or facial geometry.[7d] However, at this stage, there are no examples of complexes supported by PNP ligands that have been shown to exist in both meridional or facial geometries either in solution or the solid state, and this type of interconversion has been rarely demonstrated for pincer ligands in general.[8] Here, we report the synthesis of a number of five-coordinate Fe complexes supported by the PNP ligand, $HN\{CH_2CH_2(PR_2)\}_2$ (R = *i*Pr (^{iPr}PNP), *t*Bu (^{tBu}PNP), or cyclohexyl (^{Cy}PNP)). Using a variety of techniques, including X-ray crystallography and Mössbauer and magnetic circular dichroism (MCD) spectroscopies, we show that these complexes exist as isomers in which the PNP ligand can be in a *pseudo*-meridional or *pseudo*-facial geometry. Our studies conclusively demonstrate that these ligands are flexible in solution, which could be a crucial factor in the reactivity of this important class of compounds.

RESULTS AND DISCUSSION

Using a modification of a procedure described by Milstein and co-workers[9] for the coordination of the pyridine-based pincer ligand 2,6-$C_5H_3N(CH_2P^iPr_2)_2$, ligands ^{iPr}PNP, ^{tBu}PNP, and ^{Cy}PNP were coordinated by heating the free ligand with anhydrous $FeCl_2$ in THF (eq 1). New pincer-supported

Received: February 23, 2014
Published: May 30, 2014

   dx.doi.org/10.1021/ic5004275 | *Inorg. Chem.* 2014, 53, 6066−6072

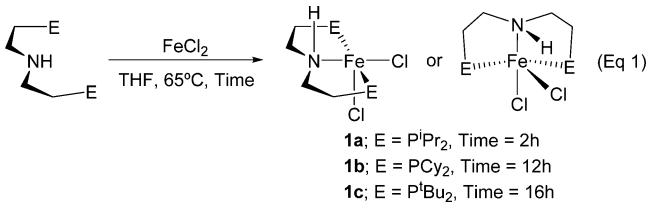

complexes **1a**–**c** are insoluble in THF and precipitate out of the reaction mixture as white solids. The reaction proceeded more slowly as the steric bulk on the phosphine substituent was increased. The coordination of the ^{iPr}PNP ligand required only 2 h to reach completion, whereas the ^{tBu}PNP and ^{Cy}PNP ligands required longer reaction times. New complexes **1a**–**c** are paramagnetic, and solution magnetic measurements using the Evans' NMR method were consistent with an S = 2 ground state for each complex. Complexes **1a** and **1c** were characterized by X-ray crystallography. Interestingly, two different solvomorphs of complex **1a** were crystallized, as shown in Figure 1. In one solvomorph, the Fe center is in a distorted square pyramidal geometry (**1a**^{spy}) and there is one acetonitrile molecule in the crystal lattice, whereas in the other solvomorph, the Fe is in a distorted trigonal bipyramidal geometry (**1a**^{tbp}). In **1a**^{spy}, the ^{iPr}PNP ligand is coordinated in the expected meridional fashion and occupies positions around the base of the square pyramid, with one of the chloride ligands occupying the axial position. The P(1)–Fe(1)–P(2) bond angle is 151.60(4)°. The degree of distortion from square pyramidal was quantified by calculating the value τ.[10] On the scale of 0 to 1, where 0 denotes idealized square pyramidal character and 1 denotes idealized trigonal bipyramidal character, τ is 0.053. In contrast, in **1a**^{tbp} the ^{iPr}PNP ligand coordinates facially and the P(1)–Fe(1)–P(2) bond angle is 117.96(4)°, whereas the angle between the nitrogen atom of the ^{iPr}PNP ligand, Fe(1) and Cl(2), which occupies one of the apical positions, is 170.19(8)°. The value of τ is 0.79. Previously facial coordination of the PNP ligand has been observed mainly in dimeric species,[7d,h,i,u] although the reported structure of (^{iPr}PNP)$CoCl_2$ is quite similar to that of **1a**^{tbp}.[7h] The Fe(1)–N(1) bond distance is significantly elongated in **1a**^{tbp} (2.372(4) Å) compared to that in **1a**^{spy} (2.260(4) Å), whereas the Fe–P bond lengths are elongated in **1a**^{spy} (2.5506(11) and 2.5853(11) Å) compared to those in **1a**^{tbp} (2.4976(9) and 2.4857(9) Å). In both cases, this is probably related to the *trans*-influence. In **1a**^{tbp}, the central nitrogen atom of the ^{iPr}PNP ligand is directly opposite a chloride ligand, whereas in **1a**^{spy}, it is not directly opposite any ligand. However, in **1a**^{spy}, the two phosphorus atoms are *trans* to each other, whereas in **1a**^{tbp}, they are not *trans* to any ligand.

In general, for simple five-coordinate (5C) transition metal compounds the potential energy surface is quite flat, and the energy difference between trigonal bipyramidal and square pyramidal geometries can be small.[11] For example, both trigonal bipyramidal and square pyramidal isomers of the simple coordination compound, $Ni(CN)_5^{3-}$, are observed in the same unit cell.[12] In contrast, for pincer complexes this type of behavior has been rarely observed. The structures of **1a**^{spy} and **1a**^{tbp} are the first examples of the same complex crystallizing with the PNP ligand in both meridional and facial geometries, and they are one of only three examples with any kind of pincer ligand.[8] In the solid state, a potential cause for the observation of both isomers could be related to hydrogen bonding, as opposed to similarities in energy between the square pyramidal and trigonal bipyramidal conformations. In **1a**^{spy}, there is a weak hydrogen-bonding interaction between the acetonitrile molecule of crystallization and one of the chloride ligands, whereas in both structures there is hydrogen bonding between the N–H group of the ligand and one of the chloride ligands (see the Supporting Information for more details). However, DFT calculations[13] in the gas phase (where there are no hydrogen bonding or packing effects) at the m06l level located two minimum energy structures, which gave reasonably good agreement with **1a**^{spy} and **1a**^{tbp} without the use of any constraints or the incorporation of acetonitrile. The

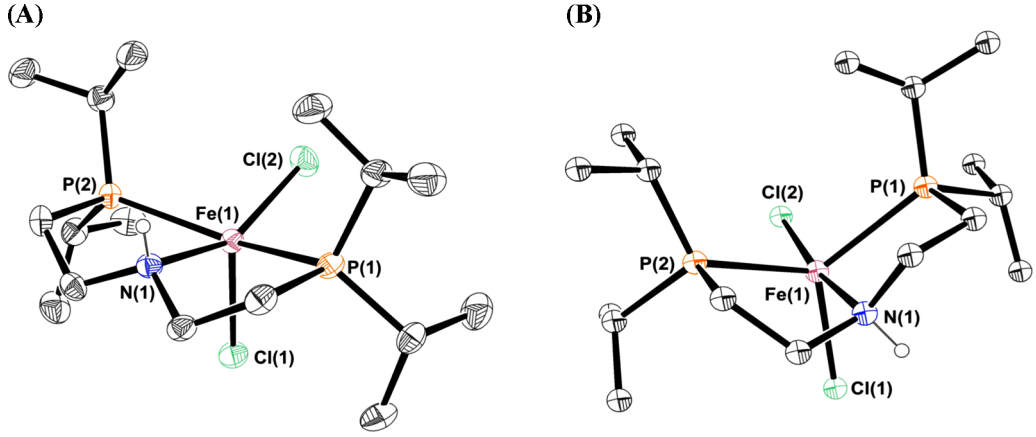

Figure 1. (A) ORTEP of **1a**^{spy} (selected hydrogen atoms and solvent of crystallization have been omitted for clarity). Selected bond lengths (angstroms) and angles (deg) are as follows: Fe(1)–Cl(1) 2.3678(10), Fe(1)–Cl(2) 2.3033(11), Fe(1)–N(1) 2.255(3), Fe(1)–P(1) 2.5506(11), Fe(1)–P(2) 2.5853(11), P(1)–Fe(1)–P(2) 151.60(4), P(1)–Fe(1)–Cl(1) 99.08(4), P(1)–Fe(1)–Cl(2) 96.56(4), P(1)–Fe(1)–N(1) 78.12(8), P(2)–Fe(1)–Cl(1) 99.77(4), P(2)–Fe(1)–Cl(2) 95.87(4), P(2)–Fe(1)–N(1) 77.93(8), Cl(1)–Fe(1)–Cl(2) 111.92(4), N(1)–Fe(1)–Cl(1) 99.66(8), N(1)–Fe(1)–Cl(2) 148.42(8). (B) ORTEP of **1a**^{tbp} (selected hydrogen atoms have been omitted for clarity). Selected bond lengths (angstroms) and angles (deg) are as follows: Fe(1)–Cl(1) 2.3390(8), Fe(1)–Cl(2) 2.3338(9), Fe(1)–N(1) 2.373(2), Fe(1)–P(1) 2.4976(9), Fe(1)–P(2) 2.4857(9), P(1)–Fe(1)–P(2) 118.03(3), P(1)–Fe(1)–Cl(1) 122.98(3), P(1)–Fe(1)–Cl(2) 94.78(3), P(2)–Fe(1)–N(1) 76.83(7), P(2)–Fe(1)–Cl(1) 109.49(3), P(2)–Fe(1)–Cl(2) 102.17(3), P(2)–Fe(1)–N(1) 77.82(7), Cl(1)–Fe(1)–Cl(2) 104.52(3), N(1)–Fe(1)–Cl(1) 84.58(6), N(1)–Fe(1)–Cl(2) 170.15(7).

dx.doi.org/10.1021/ic5004275 | *Inorg. Chem.* 2014, 53, 6066–6072

calculated structure of **1a**^{spy} is 0.73 kJ mol^{-1} lower in energy than that of the calculated structure of **1a**^{tbp}, and similar results were obtained with the uB3LYP functional. This suggests that although packing effects (see Supporting Information for more details) in the solid state could be responsible for the observation of both isomers using X-ray crystallography, the energy difference between the trigonal bipyramidal and square pyramidal forms of **1a** is small and both isomers might be present in solution. This is explored further using MCD spectroscopy (*vide infra*).

The crystal structure of **1c** is essentially isostructural with that of **1a**^{spy} (Figure 2). The ^{tBu}PNP ligand is coordinated in a

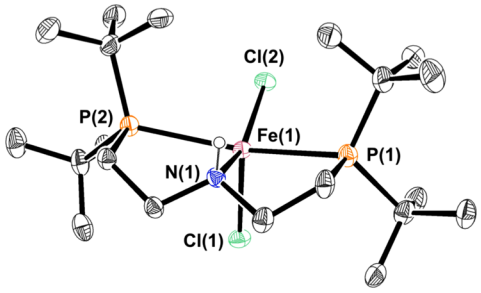

Figure 2. ORTEP of **1c** (selected hydrogen atoms have been omitted for clarity). Selected bond lengths (angstroms) and angles (deg) are as follows: Fe(1)−Cl(1) 2.3334(14), Fe(1)−Cl(2) 2.3385(11), Fe(1)−N(1) 2.221(3), Fe(1)−P(1) 2.6144(15), Fe(1)−P(2) 2.6111(14), P(1)−Fe(1)−P(2) 150.33(4), P(1)−Fe(1)−Cl(1) 100.75(5), P(1)−Fe(1)−Cl(2) 97.81(4), P(1)−Fe(1)−N(1) 78.15(10), P(2)−Fe(1)−Cl(1) 100.02(5), P(2)−Fe(1)−Cl(2) 96.13(4), P(2)−Fe(1)−N(1) 77.35(10), Cl(1)−Fe(1)−Cl(2) 106.95(4), N(1)−Fe(1)−Cl(1) 100.70(11), N(1)−Fe(1)−Cl(2) 152.30(11).

meridional fashion (the P(1)−Fe(1)−P(2) angle is 150.33(4)°), and the Fe center is in a distorted square pyramidal geometry (the value of τ is 0.033). A structural overlay of **1a**^{spy} and **1c** reveals that the extra methyl groups present on ^{tBu}PNP compared with ^{iPr}PNP occupy space above the open coordination site of **1c**.[13] This pushes Cl(2) away from the open site, and the Cl(1)−Fe(1)−Cl(2) bond angle is more acute in **1c** (106.95(4)°) compared with that in **1a**^{spy} (111.97(5)°).

^{57}Fe Mössbauer spectroscopy was performed to investigate the electronic structures of as-isolated powder samples of **1a**−**c** in the solid state (Figure 3). In all cases, the samples were not exposed to acetonitrile. The 80 K Mössbauer spectrum of **1a** (Figure 3A) is well-fit to a single Fe species, with δ = 0.86 mm/s and ΔE_Q = 2.89 mm/s. For **1b** (Figure 3B), the best fit to the 80 K Mössbauer data comprises a single major component, with δ = 0.86 mm/s and ΔE_Q = 2.98 mm/s (∼97% of all Fe, red component). A minor species, which has parameters in the expected range for a potential Fe(III) impurity, is also present (δ = 0.46 mm/s, ΔE_Q = 0.69 mm/s, ∼ 3% of all Fe, blue component). The 80 K Mössbauer spectrum of **1c** (Figure 3C) is well-fit to a single Fe species, with δ = 0.99 mm/s and ΔE_Q = 2.69 mm/s. The observed isomer shifts for the three (PNP)FeCl$_2$ complexes all fall in the range of 0.85−1.0 mm/s, consistent with the presence of high-spin, S = 2 Fe(II) species.[14] By comparison, the high-spin S = 2 distorted square pyramidal (PN^{Py}P)FeCl$_2$ complex (PN^{Py}P = 2,6-C$_5$H$_3$N-(CH$_2$P^{i}Pr$_2$)$_2$, where a pyridine forms the central part of the pincer ligand) has Mössbauer parameters of δ = 0.80 mm/s and ΔE_Q = 2.56 mm/s.[14c] It is notable that although the Mössbauer

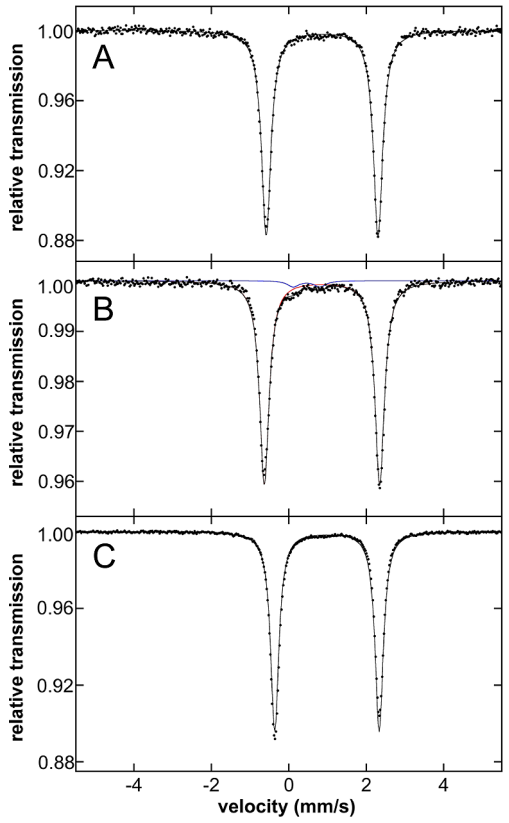

Figure 3. ^{57}Fe Mössbauer (80 K) data (black dots) and fit (black lines) of solid powders of (A) (^{iPr}PNP)FeCl$_2$ (**1a**), (B) (^{Cy}PNP)FeCl$_2$ (**1b**), and (C) (^{tBu}PNP)FeCl$_2$ (**1c**). For **1b**, both major and minor components are present in the best fit, as described in the text.

parameters of **1a** and **1b** are very similar, **1c** exhibits a higher isomer shift (0.99 vs 0.86 mm/s; error in δ is ±0.02 mm/s) as well as a smaller quadrupole splitting (2.69 vs 2.89 mm/s; error in ΔE_Q ± 0.04 mm/s). These differences are further demonstrated by a direct overlay comparison of the spectra of **1a** and **1c** (see Supporting Information, Figure S1). This variation suggests the possible presence of a different structural distortion for **1c** in the solid-state powder, which is more rigorously determined by direct evaluation of the observed differences in the d−d transitions of the powders in NIR MCD spectroscopy (*vide infra*). Lastly, no contributions of minor species corresponding to a second iron(II) 5C species are observed in the solid-state spectra. Consistent with this, there is also no evidence of a second species from the d−d transitions observed of the same solid samples in NIR MCD (*vide infra*). If present, such a minor species is below our detectable limit and would represent approximately <1−2% of all iron present.

Near-infrared (NIR) MCD studies were performed on the solid-state powder samples used for Mössbauer spectroscopy in order to probe the electronic and geometric structures of **1a**−**c** further (Figure 4). The 5 K, 7 T NIR MCD spectrum of a mull of **1a** (Figure 4A) exhibits two ligand-field (LF) transitions at <5000 and 10 560 cm^{-1}. A very similar set of LF transitions are also observed in the 5 K, 7 T NIR MCD spectrum of a mull of **1b** (bands at <5000 and 10 770 cm^{-1}). In contrast, the 5 K, 7 T NIR MCD spectrum of **1c** exhibits only a single LF transition at 9260 cm^{-1}. Importantly, the energies of the observed LF transitions can be directly related to the coordination number and geometry of the Fe(II) complexes.[15] For a S = 2 Fe(II) 5C complex, the LF splittings have been previously quantified

dx.doi.org/10.1021/ic5004275 | Inorg. Chem. 2014, 53, 6066−6072

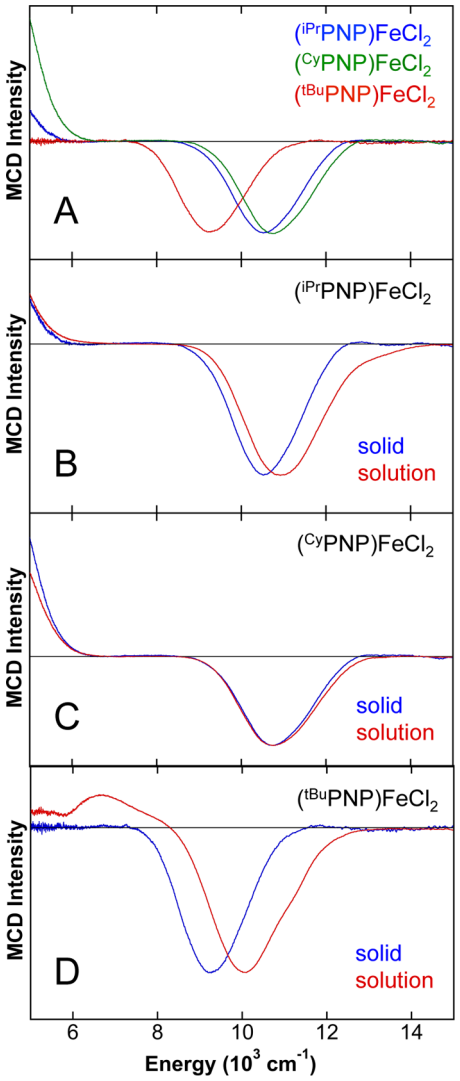

Figure 4. NIR MCD spectra (5 K, 7 T) of $(PNP)FeCl_2$ complexes. (A) NIR MCD of solid-state mulls of $(^{iPr}PNP)FeCl_2$ (**1a**), $(^{Cy}PNP)FeCl_2$ (**1b**), and $(^{tBu}PNP)FeCl_2$ (**1c**). (B–D) Comparison of solid-state mull and frozen solution glasses (1:1 DCM-d_2/toluene-d_8) NIR MCD spectra of (B) $(^{iPr}PNP)FeCl_2$ (**1a**), (C) $(^{Cy}PNP)FeCl_2$ (**1b**), and (D) $(^{tBu}PNP)FeCl_2$ (**1c**). See the Supporting Information for peak fits to the individual components present in the observed mixtures in solution.

using both LF theory calculations and MCD measurements of well-defined coordination complexes with nitrogen and oxygen ligands. In distorted square pyramidal 5C Fe(II) (S = 2) complexes, the ^5E state splits by ~5000 cm^{-1}, resulting in two LF transitions at >10 000 cm^{-1} and ~5000 cm^{-1}.[15c−e] By comparison, distortion to a trigonal bipyramidal 5C structure leads to a smaller LF with transitions at <10 000 and <5000 cm^{-1}.[15c−e] Importantly, the MCD model studies of 5C iron(II) complexes also demonstrated that changes in bond lengths and/or distortions of square pyramidal structures can result in significant changes in the highest energy LF transition via stabilization/destabilization of d_{x2-y2}.[15c] For example, changes in the strength of axial M−L bonding (via substitution of Cl for Br) shifts iron out of the *xy* plane and stabilizes x^2-y^2, resulting in an increase in highest energy LF transitions by ~800 cm^{-1} for $[Fe(TMC)Cl]^+$ versus $Fe(TMC)Br]^+$ (TMC = 1,4,8,11-tetramethyl-1,4,8,11-tetraazacyclotetradecane). Furthermore, these studies demonstrated the sensitivity of x^2-y^2 to changes in the equatorial plane because of differences in LF strength, where differences of up to 1800 cm^{-1} were observed for Fe−O ligation in the equatorial plane by changing the bidentate oxygen donor across OAc, OBz, and acac. Differences in LF strength can also occur because of changes in M−L bond distances. This LF analysis of geometries and structural distortions based on NIR MCD measurements has been successfully applied previously to several iron(II) 5C species, including very low symmetry sites in nonheme iron metalloenzymes.[15d,e]

Although direct measurements of LF transition energies in 5C, high-spin S = 2 Fe complexes supported by PNP ligands have not been reported, the combination of equal numbers of stronger field phosphine ligands and weaker field chloride ligands would be anticipated to result in LF energies for the $(PNP)FeCl_2$ complexes of comparable magnitude to those previously reported for the N/O-ligated complexes (as is observed from MCD in Figure 4). Thus, within a series of related $(PNP)FeCl_2$ complexes, the extent of distortion toward a square pyramidal versus a trigonal bipyramidal structure can be evaluated using the observed LF energies. The observed LF transitions for **1a** (Figure 4A, blue) at 10 560 cm^{-1} and a low energy tail at <5000 cm^{-1} are consistent with $(^{iPr}PNP)FeCl_2$ (**1a**) being a single 5C, high-spin Fe(II) species with a geometric perturbation toward a distorted square pyramidal structure, one of the structures observed by crystallography. There is no evidence for a second iron species such as the distorted TBP structure, which was also characterized by crystallography, presumably because of the different conditions used for the growth of single crystals compared to precipitation of a powder. Although no crystal structure was obtained for $(^{Cy}PNP)FeCl_2$ (**1b**), the LF transitions observed in the solid state for this complex (Figure 4B, green) are nearly identical to those of **1a** and are also consistent with a single 5C, high-spin Fe(II) species with a distorted square pyramidal structure. In contrast to complexes **1a** and **1b**, $(^{tBu}PNP)FeCl_2$ (**1c**, Figure 4C, red) contains only a single observable LF transition at lower energy (9260 cm^{-1}), consistent with a different structural distortion of this 5C Fe(II) complex in the solid-state powder. Although the observed lower energy LF transition might suggest distortion to a TBP geometry, variable-temperature variable-field MCD indicates that **1c** has a +ZFS S = 2 ground-state (see Supporting Information, Figure S2A), which is not consistent with a TBP ground state that requires a −ZFS ground state[15a] (by contrast, the saturation magnetization data for **1a** and **1b** are highly similar, see Supporting Information, Figure S2B). Thus, **1c** is best described as a 5C complex distorted away from SP geometry. The significant differences in the LF energy for the highest energy transitions (~1300 cm^{-1} lower in energy for **1c**) can be evaluated in terms of structural distortions that lower the energy of x^2-y^2. The presence of the sterically bulky *t*Bu substituents on the PNP ligand could lead to increased Fe−P bond lengths in the *xy* plane (as observed in the SP crystal structure of **1c**) and would serve to stabilize x^2-y^2. Alternatively, movement of the phosphorus ligands out of the *xy* plane would also stabilize x^2-y^2, where this structural distortion would represent a more significant distortion away from SP and could also result from the increased steric bulk of the *t*Bu substituents. Both distortions are likely present in **1c** in the solid powder in order to generate the large observed reduction in energy of x^2-y^2 determined by NIR MCD.

dx.doi.org/10.1021/ic5004275 | Inorg. Chem. 2014, 53, 6066−6072

Although the X-ray data and NIR MCD spectra define the LF energies and hence the structures and distortions present in solid-state crystals and powders of the Fe complexes, respectively, these studies provide no information about the speciation in solution, which is almost certainly more important for reactivity. In order to understand the structures of **1a**–**c** in solution, analogous NIR MCD studies were performed on frozen solution samples (in 1:1 DCM-d_2/toluene-d_8). For (^{iPr}PNP)FeCl$_2$ (**1a**, Figure 4B, red), the solution NIR MCD spectrum indicates the presence of LF bands at <5000, 10 900, and 12 580 cm^{-1} (see Supporting Information Figure S3 for peak fit analysis). The presence of the weak transition at 12 580 cm^{-1} is further demonstrated by variable-field MCD experiments (see Supporting Information, Figure S4). Because LF theory dictates that a single Fe(II) (S = 2) complex can exhibit only two LF transitions, the presence of three LF bands indicates the presence of two distinct structural distortions in solution. On the basis of the energies of the two highest energy LF transitions, both species are consistent with distortion toward square pyramidal 5C species. Interestingly, the energies of these transitions (10 900 and 12 580 cm^{-1}) are both increased compared to those in the solid-state powder, consistent with an increased LF because of stronger Fe–L bonding interactions in solution and/or distortions of the complex to destabilize x^2-y^2 (for example, a more planar equatorial plane). Overall, these results suggest that the ^{iPr}PNP ligand is able to stabilize two different distorted 5C structures of **1a** in solution, although unlike the solid-state results, where both *pseudo*-square pyramidal and *pseudo*-trigonal bipyramidal isomers are observed, it appears that only more square pyramidal species are present in solution. In contrast, the solution NIR MCD spectrum of **1b** (Figure 4C, red) contains only two LF transitions (at <5000 and 10 770 cm^{-1}), identical to the energies observed for **1b** in the solid-state mull, indicating the presence of a single distorted square pyramidal species that is unchanged between the solution and solid states. Notably, the solution MCD spectrum of **1c** (Figure 4D, red) shows a dramatic change relative to the mull spectrum (Figure 4D, blue), with the presence of three distinct LF transitions indicating the presence of at least two different Fe species in solution (see Supporting Information Figure S3 for peak fit analysis). Two high-energy transitions at 9980 and 11 140 cm^{-1} are present, both of which are higher in energy than the transition observed in the mull at 9260 cm^{-1}. An additional LF band is also present in solution at 6770 cm^{-1}. The dramatic changes in the LF transition energies of **1c** in solution indicate significant structural perturbations of **1c**, reflecting the flexibility of this PNP complex. The Fe(II) species present in solution are best described as a distorted square pyramidal complex (11 140 cm^{-1} band) as well as a species (9890 cm^{-1} band) with a reduced LF energy, which is likely due to the potential distortions previously discussed for **1c** in the solid state (vide supra). Importantly, the NIR MCD data for **1c** demonstrates the significant structural changes that are possible in Fe(II) complexes supported by PNP ligands between solid state and solution environments and indicates that the PNP ligand in **1c** does not bind in the rigid fashion often invoked for pincer-supported complexes.

CONCLUSIONS

We have demonstrated that PNP-type pincer ligands are flexible both in solution and the solid state, providing further support for the hypothesis that the use of alkyl linkers in pincer ligands generates systems that are not rigid. We believe that there is a link between the flexibility of the ligand and the substituents on the ligand, although how these properties are related remains to be established. Future work will also aim to determine if there is a correlation between flexibility and reactivity.

EXPERIMENTAL SECTION

General Methods. Experiments were performed under a dinitrogen or argon atmosphere in an M-Braun drybox or using standard Schlenk techniques unless otherwise noted. Under standard glovebox conditions, purging was not performed between uses of pentane, diethyl ether, benzene, toluene, and THF; thus when any of these solvents were used, traces of all of these solvents were in the atmosphere. Moisture- and air-sensitive liquids were transferred by stainless steel cannula on a Schlenk line or in a drybox. The solvents for air- and moisture-sensitive reactions were dried by passage through a column of activated alumina followed by storage under dinitrogen or argon. All commercial chemicals were used as received except where noted. ^{iPr}PNP,[7c] ^{Cy}PNP,[16] and ^{tBu}PNP[7m] were prepared using literature procedures. Anhydrous FeCl$_2$ was purchased from Aldrich and used as received. IR spectra were measured using a diamond smart orbit ATR on a Nicolet 6700 FT-IR instrument. Solution magnetic susceptibilities were determined by ^{1}H NMR spectroscopy using the Evans' method.[17] Robertson Microlit Laboratories, Inc. performed the elemental analyses (inert atmosphere).

Experimental Procedures and Characterizing Data for New Compounds. *(^{iPr}PNP)FeCl$_2$ (**1a**).* To a suspension of 206 mg of anhydrous FeCl$_2$ (1 equiv, 1.6 mmol) in 7 mL of THF was added 500 mg of bis(diisopropylphosphinoethyl)amine (1 equiv, 1.6 mmol) at 25 °C. The solution was heated at reflux for 2 h, during which time **1a** precipitated as a white crystalline powder. The solution was allowed to cool to room temperature, and the solid was isolated by filtration. Crystals suitable for X-ray diffraction were grown from a saturated ACN solution at −30 °C or a saturated THF solution at −30 °C. Yield: 0.670g (1.5 mmol, 93%).

Anal. Found (Calcd) for C$_{16}$H$_{37}$Cl$_2$FeNP$_2$: C, 44.50 (44.47); H, 8.81 (8.63); N, 3.44 (3.24). Magnetic susceptibility (CD$_2$Cl$_2$): 5.54μ_B. IR (cm^{-1}): 3240, 2951, 2932, 2867, 1462, 1421, 1407, 1390, 1370, 1301, 1240, 1220, 1183, 1159, 1092, 1045, 929, 897, 821, 764, 692, 667, 640, 615, 549.

*(^{Cy}PNP)FeCl$_2$ (**1b**).* To a solution of 740 mg of bis-(dicyclohexylphosphinoethyl)amine (1 equiv, 1.5 mmol) in 15 mL of THF was added 200 mg of anhydrous FeCl$_2$ (1 equiv, 1.5 mmol) at 25 °C. The solution was heated at reflux for 4 h, during which time **1b** precipitated as a white crystalline powder. The solution was allowed to cool to room temperature, and **1b** was then isolated by filtration. Yield: 350 mg (0.5 mmol, 33%).

Anal. Found (Calcd): C, 56.14 (56.77); H, 8.61 (9.02); N, 2.26 (2.36). Magnetic susceptibility (CD$_2$Cl$_2$): 5.27μ_B. IR (cm^{-1}): 3242, 2922, 2850, 1445, 1098, 1000, 884, 855, 800, 739, 672, 562, 511.

*(^{tBu}PNP)FeCl$_2$ (**1c**).* To a solution of 1 g of bis-(ditertbutylphosphinoethyl)amine (1 equiv, 3.06 mmol) in 6 mL of THF was added 386 mg (1 equiv, 3.06 mmol) of anhydrous FeCl$_2$ at 25 °C. The solution was heated at reflux for 16 h, during which time **1c** precipitated as a white crystalline powder. The solution was allowed to cool to room temperature, and the solid was then isolated by filtration. Crystals suitable for X-ray diffraction were grown from a saturated ACN/THF solution at −30 °C. Yield: 1.00 g (2 mmol, 74%).

Anal. Found (Calcd) for C$_{20}$H$_{45}$Cl$_2$FeNP$_2$: C, 49.14 (49.20); H, 9.47 (9.29); N, 2.88 (2.87). Magnetic susceptibility (CD$_2$Cl$_2$): 5.34μ_B. IR (cm^{-1}): 3216, 2937, 2863, 1479, 1467, 1389, 1369, 1176, 1129, 1076, 1054, 1020, 971, 933, 826, 813, 769, 690, 601, 577, 506.

X-ray Crystallography. Crystal samples were mounted in MiTeGen polyimide loops with immersion oil. Low-temperature diffraction data (ω scans) were collected on either a Rigaku SCXMini diffractometer with a Rigaku CCD detector using filtered Mo Kα radiation (λ = 0.71073 Å) for **1a**^{spy} and **1a**^{tbp} or a Rigaku MicroMax-007HF

dx.doi.org/10.1021/ic5004275 | Inorg. Chem. 2014, 53, 6066–6072

diffractometer coupled to a Saturn994+ CCD detector with Cu Kα radiation (λ = 1.54178 Å) for **1c**. All structures were solved by direct methods using SHELXS[18] and refined against F^2 on all data by full-matrix least-squares with SHELXL-97[19] using established refinement techniques.[20] All hydrogen atoms were included into the model at geometrically calculated positions and refined using a riding model. The isotropic displacement parameters of all hydrogen atoms were fixed to 1.2 times the U value of the atoms to which they are linked (1.5 times for methyl groups).

^{57}Fe Mössbauer Spectroscopy. All solid samples for ^{57}Fe Mössbauer spectroscopy were run on nonenriched samples of the as-isolated samples. All samples were prepared in an inert atmosphere glovebox equipped with a liquid nitrogen fill port to enable sample freezing to 77 K within the glovebox. Each sample was loaded into a Delrin Mössbauer sample cup for measurements and loaded under liquid nitrogen. Low-temperature Mössbauer measurements were performed using a See Co. MS4 Mössbauer spectrometer integrated with a Janis SVT-400T He/N_2 cryostat for measurements at 80 K with a 0.07 T applied magnetic field. Isomer shifts were determined relative to α-Fe at 298 K. All Mössbauer spectra were fit using the program WMoss (SeeCo). The errors for the Mössbauer parameters for the multicomponent fits are as follows: δ (±0.02 mm/s), ΔE_Q (±0.04 mm/s), and percent contribution (±3%).

Magnetic Circular Dichroism Spectroscopy. All samples for MCD spectroscopy were prepared in an inert atmosphere glovebox equipped with a liquid nitrogen fill port to enable sample freezing to 77 K within the glovebox. MCD measurements of solid powders were performed on mulls prepared with fluorolube. Solution MCD samples were prepared in 1:1 (v/v) DCM-d_2/toluene-d_8 (to form low-temperature optical glasses) in copper cells fitted with quartz disks and a 3 mm gasket. All solution measurements were performed on ∼3 mM solutions of the corresponding (PNP)$FeCl_2$ complex. Low-temperature near-infrared (NIR) MCD data were collected with a Jasco J-730 spectropolarimeter and a liquid nitrogen-cooled InSb detector. The MCD instrument utilizes a modified sample compartment incorporating focusing optics and an Oxford Instruments SM4000-7T superconducting magnet/cryostat. This setup permits measurements from 1.6 to 290 K with magnetic fields up to 7 T. A calibrated Cernox sensor directly inserted in the copper sample holder is used to measure the temperature at the sample to 0.001 K. All MCD spectra were baseline-corrected against zero-field scans.

■ ASSOCIATED CONTENT

Ⓢ Supporting Information

Mössbauer and MCD spectra; X-ray information for **1a^{spy}**, **1a^{tbp}**, and **1c**; and details about DFT calculations including optimized structures and energies. This material is available free of charge via the Internet at http://pubs.acs.org.

■ AUTHOR INFORMATION

Corresponding Authors

*(N.H.) E-mail: nilay.hazari@yale.edu.

*(M.L.N.) E-mail: neidig@chem.rochester.edu.

Author Contributions

§These authors made equal contributions.

Notes

The authors declare no competing financial interest.

■ ACKNOWLEDGMENTS

N.H. thanks the National Science Foundation for support through grant CHE-1240020, a Center for Chemical Innovation, and M.L.N. acknowledges the University of Rochester for the start-up funding used to support this work. N.H. is a fellow of the Alfred P. Sloan Foundation. In addition, this work was supported in part by the facilities and staff of the Yale University Faculty of Arts and Sciences High Performance Computing Center and by the National Science Foundation under grant no. CNS 08-21132, which partially funded acquisition of the facilities. C.J.P. gratefully acknowledges funding from the STARS II program at Yale University. We thank Dr. Brandon Mercado for providing assistance with the interpretation of X-ray crystallographic data.

■ REFERENCES

(1) (a) Albrecht, M.; van Koten, G. *Angew. Chem., Int. Ed.* **2001**, *40*, 3750. (b) van der Boom, M. E.; Milstein, D. *Chem. Rev.* **2003**, *103*, 1759. (c) Leis, W.; Mayer, H. A.; Kaska, W. C. *Coord. Chem. Rev.* **2008**, *252*, 1787. (d) Benito-Garagorri, D.; Kirchner, K. *Acc. Chem. Res.* **2008**, *41*, 201. (e) Selander, N.; J. Szabó, K. *Chem. Rev.* **2010**, *111*, 2048. (f) Albrecht, M.; Lindner, M. M. *Dalton Trans.* **2011**, *40*, 8733.

(2) (a) McLoughlin, M. A.; Keder, N. L.; Harrison, W. T. A.; Flesher, R. J.; Mayer, H. A.; Kaska, W. C. *Inorg. Chem.* **1999**, *38*, 3223. (b) Tanaka, R.; Yamashita, M.; Nozaki, K. *J. Am. Chem. Soc.* **2009**, *131*, 14168. (c) Chakraborty, S.; Zhang, J.; Krause, J. A.; Guan, H. *J. Am. Chem. Soc.* **2010**, *132*, 8872. (d) Langer, R.; Diskin-Posner, Y.; Leitus, G.; Shimon, L. J. W.; Ben-David, Y.; Milstein, D. *Angew. Chem., Int. Ed.* **2011**, *50*, 9948.

(3) (a) Arashiba, K.; Miyake, Y.; Nishibayashi, Y. *Nat. Chem.* **2011**, *3*, 120. (b) Arashiba, K.; Sasaki, K.; Kuriyama, S.; Miyake, Y.; Nakanishi, H.; Nishibayashi, Y. *Organometallics* **2012**, *31*, 2035. (c) Hebden, T.; Schrock, R.; Takase, M.; Müller, P. *Chem. Commun.* **2012**, *48*, 1851.

(4) Choi, J.; MacArthur, A. H. R.; Brookhart, M.; Goldman, A. S. *Chem. Rev.* **2011**, *111*, 1761.

(5) (a) McGuinness, D. S.; Gibson, V. C.; Wass, D. F.; Steed, J. W. *J. Am. Chem. Soc.* **2003**, *125*, 12716. (b) Britovsek, G. J. P.; Bruce, M.; Gibson, V. C.; Kimberley, B. S.; Maddox, P. J.; Mastroianni, S.; McTavish, S. J.; Redshaw, C.; Solan, G. A.; Stroemberg, S.; White, A. J. P.; Williams, D. J. *J. Am. Chem. Soc.* **1999**, *121*, 8728. (c) Small, B. L.; Brookhart, M.; Bennett, A. M. A. *J. Am. Chem. Soc.* **1998**, *120*, 4049.

(6) Poyatos, M.; Mata, J. A.; Falomir, E.; Crabtree, R. H.; Peris, E. *Organometallics* **2003**, *22*, 1110.

(7) (a) Danopoulos, A. A.; Edwards, P. G. *Polyhedron* **1989**, *8*, 1339. (b) Danopoulos, A. A.; Edwards, P. G.; Parry, J. S.; Wills, A. R. *Polyhedron* **1989**, *8*, 1767. (c) Danopoulos, A. A.; Wills, A. R.; Edwards, P. G. *Polyhedron* **1990**, *9*, 2413. (d) Bianchini, C.; Innocenti, P.; Peruzzini, M.; Romerosa, A.; Zanobini, F. *Organometallics* **1996**, *15*, 272. (e) Clarke, Z. E.; Maragh, P. T.; Dasgupta, T. P.; Gusev, D. G.; Lough, A. J.; Abdur-Rashid, K. *Organometallics* **2006**, *25*, 4113. (f) Choualeb, A.; Lough, A. J.; Gusev, D. G. *Organometallics* **2007**, *26*, 3509. (g) Bertoli, M.; Choualeb, A.; Lough, A. J.; Moore, B.; Spasyuk, D.; Gusev, D. G. *Organometallics* **2011**, *30*, 3479. (h) Rozenel, S. S.; Kerr, J. B.; Arnold, J. *Dalton Trans.* **2011**, *40*, 10397. (i) Rozenel, S. S.; Arnold, J. *Inorg. Chem.* **2012**, *51*, 9730. (j) McGuinness, D. S.; Wasserscheid, P.; Keim, W.; Hu, C.; Englert, U.; Dixon, J. T.; Grove, C. *Chem. Commun.* **2003**, 334. (k) McGuinness, D. S.; Wasserscheid, P.; Morgan, D. H.; Dixon, J. T. *Organometallics* **2005**, *24*, 552. (l) Schmeier, T. J.; Dobereiner, G. E.; Crabtree, R. H.; Hazari, N. *J. Am. Chem. Soc.* **2011**, *133*, 9274. (m) Meiners, J.; Friedrich, A.; Herdtweck, E.; Schneider, S. *Organometallics* **2009**, *28*, 6331. (n) Kaess, M.; Friedrich, A.; Drees, M.; Schneider, S. *Angew. Chem., Int. Ed.* **2009**, *48*, 905. (o) Friedrich, A.; Ghosh, R.; Kolb, R.; Herdtweck, E.; Schneider, S. *Organometallics* **2009**, *28*, 708. (p) Marziale, A. N.; Herdtweck, E.; Eppinger, J.; Schneider, S. *Inorg. Chem.* **2009**, *48*, 3699. (q) Friedrich, A.; Drees, M.; Schneider, S. *Chem.—Eur. J.* **2009**, *15*, 10339. (r) Friedrich, A.; Drees, M.; auf der Günne, J. S.; Schneider, S. *J. Am. Chem. Soc.* **2009**, *131*, 17552. (s) Askevold, B.; Khusniyarov, M. M.; Herdtweck, E.; Meyer, K.; Schneider, S. *Angew. Chem., Int. Ed.* **2010**, *49*, 7566. (t) Askevold, B.; Nieto, J.; Tussupbayev, S.; Diefenbach, M.; Herdtweck, E.; Holthausen, M.; Schneider, S. *Nat. Chem.* **2011**, *3*, 532. (u) Friedrich, A.; Drees, M.; Käss, M.; Herdtweck, E.; Schneider, S. *Inorg. Chem.* **2010**, *49*, 5482. (v) Meiners, J.; Scheibel, M. G.; Lemee-Cailleau, M.-H.; Mason, S. A.; Boeddinghaus, M. B.; Faessler, T. F.; Herdtweck, E.; Khusniyarov, M. M.; Schneider, S. *Angew. Chem., Int. Ed.* **2011**, *50*,

8184. (w) Scheibel, M. G.; Askevold, B.; Heinemann, F. W.; Reijerse, E. J.; de Bruin, B.; Schneider, S. *Nat. Chem.* **2012**, *4*, 552. (x) Schneider, S.; Meiners, J.; Askevold, B. *Eur. J. Inorg. Chem.* **2012**, *2012*, 412. (y) Scheibel, M. G.; Wu, Y.; Stückl, A. C.; Krause, L.; Carl, E.; Stalke, D.; de Bruin, B.; Schneider, S. *J. Am. Chem. Soc.* **2013**, *135*, 17719. (z) Marziale, A. N.; Friedrich, A.; Klopsch, I.; Drees, M.; Celinski, V. R.; auf der Günne, J. S.; Schneider, S. *J. Am. Chem. Soc.* **2013**, *135*, 13342. (aa) Koehne, I.; Schmeier, T. J.; Bielinski, E. A.; Pan, C. J.; Lagaditis, P. O.; Bernskoetter, W. H.; Takase, M. K.; Würtele, C.; Hazari, N.; Schneider, S. *Inorg. Chem.* **2014**, *53*, 2133. (ab) Nielsen, M.; Alberico, E.; Baumann, W.; Drexler, H.-J.; Junge, H.; Gladiali, S.; Beller, M. *Nature* **2013**, *495*, 85. (ac) Alberico, E.; Sponholz, P.; Cordes, C.; Nielsen, M.; Drexler, H.-J.; Baumann, W.; Junge, H.; Beller, M. *Angew. Chem., Int. Ed.* **2013**, *52*, 14162. (ad) Zhang, G.; Scott, B. L.; Hanson, S. K. *Angew. Chem., Int. Ed.* **2012**, *51*, 11907. (ae) Zhang, G.; Vasudevan, K. V.; Scott, B. L.; Hanson, S. K. *J. Am. Chem. Soc.* **2013**, *135*, 8668.

(8) To the best of our knowledge, there are no conclusive examples of complexes with any pincer ligand being shown to exist as a mixture of meridional and facial isomers in solution under thermal control. There are two examples of complexes with pincer ligands being characterized by X-ray crystallography in both the meridional and facial configurations. For an example with an NNN ligand, see: Harkins, S. B.; Peters, J. C. *Inorg. Chem.* **2006**, *45*, 4316. For an example with an SPS ligand, see: Doux, M.; Mézailles, N.; Ricard, L.; Le Floch, P.; Vaz, P. D.; Calhorda, M. J.; Mahabiersing, T.; Hartl, F. *Inorg. Chem.* **2005**, *44*, 9213 In both of these cases, conversion between the isomers occurs photochemically.

(9) Langer, R.; Leitus, G.; Ben-David, Y.; Milstein, D. *Angew. Chem., Int. Ed.* **2011**, *50*, 2120.

(10) Addison, A. W.; Rao, T. N.; Reedijk, J.; van Rijn, J.; Verschoor, G. C. *J. Chem. Soc., Dalton Trans.* **1984**, 1349.

(11) Crabtree, R. H. *The Organometallic Chemistry of the Transition Metals*, 5th ed.; Wiley: Hoboken, NJ, 2009.

(12) Muetterties, E. L.; Schunn, R. A. *Q. Rev., Chem. Soc.* **1966**, *20*, 245.

(13) See the Supporting Information for more details.

(14) (a) Gütlich, P.; Bill, E.; Trautwein, A. E.; *Mössbauer Spectroscopy and Transition Metal Chemistry: Fundamentals and Applications*; Springer-Verlag: Berlin, 2011. (b) Bart, S. C.; Chlopek, K.; Bill, E.; Bouwkamp, M. W.; Lobkovsky, E.; Neese, F.; Wieghardt, K.; Chirik, P. J. *J. Am. Chem. Soc.* **2006**, *128*, 13901. (c) Benito-Garagorri, D.; Alves, L. G.; Puchberger, M.; Mereiter, K.; Veiros, L. F.; Calhorda, M. J.; Carvalho, M. D.; Ferreira, L. P.; Godinho, M.; Kirchner, K. *Organometallics* **2009**, *28*, 6902. (d) Widger, L. R.; Jiang, Y.; Siegler, M. A.; Kumar, D.; Latifi, R.; de Visser, S. P.; Jameson, G. N. L.; Goldberg, D. P. *Inorg. Chem.* **2013**, *52*, 10467.

(15) (a) Solomon, E. I.; Pavel, E. G.; Loeb, K. E.; Campochiaro, C. *Coord. Chem. Rev.* **1995**, *144*, 369. (b) Whittaker, J. W.; Solomon, E. I. *J. Am. Chem. Soc.* **1988**, *110*, 5329. (c) Pavel, E. G.; Kitajima, N.; Solomon, E. I. *J. Am. Chem. Soc.* **1998**, *120*, 3949. (d) Solomon, E. I.; Brunold, T. C.; Davis, M. I.; Kemsley, J. N.; Lee, S.-K.; Lehnert, N.; Neese, F.; Skulan, A. J.; Yang, Y.-S.; Zhou, J. *Chem. Rev.* **2000**, *100*, 235. (e) Neidig, M. L.; Solomon, E. I. *Chem. Commun.* **2005**, 5843.

(16) Abdur-Rashid, K.; Graham, T.; Tsang, C.-W.; Chen, X.; Guo, R.; Jia, W.; Amoroso, D.; Sui-Seng, C. The Generation of Hydrogen from Ammonia Borane through Catalytic Hydrolysis. Patent WO 2008141439 A1 20081127, 2008.

(17) Evans, D. F. *J. Chem. Soc.* **1959**, 2003.

(18) Sheldrick, G. M. *Acta Crystallogr., Sect. A* **1990**, *46*, 467.

(19) Sheldrick, G. M. *Acta Crystallogr., Sect. A* **2008**, *64*, 112.

(20) Müller, P. *Crystallogr. Rev.* **2009**, *15*, 57.